

# Phenyl- versus cyclohexyl-terminated substituents: Comparative study on aggregated structures and electrontransport properties in n-type organic semiconductors

Journal:	Molecular Systems Design & Engineering			
Manuscript ID	ME-ART-07-2024-000110.R1			
Article Type:	Paper			
Date Submitted by the Author:	18-Sep-2024			
Complete List of Authors:	Kumagai, Shohei; Tokyo Institute of Technology, Department of Chemical Science and Engineering, School of Materials and Chemical Technology; The University of Tokyo, Graduate School of Advanced Materials Science, Department of Frontier Sciences Koguma, Takeru; The University of Tokyo, Graduate School of Advanced Materials Science, Department of Frontier Sciences Arai, Yutaro; The University of Tokyo Watanabe, Go; Kitasato University, Department of Physics, School of Science Ishii, Hiroyuki; University of Tsukuba Takeya, Jun; The University of Tokyo, Department of Advanced Materials Science Okamoto, Toshihiro; Tokyo Institute of Technology, Department of Chemical Science and Engineering, School of Materials and Chemical Technology			

SCHOLARONE™ Manuscripts Organic semiconductors (OSCs) offer the great opportunity of solution-processable devices, for which the molecular design involves a  $\pi$ -electron core and solubilizing side-chain substituents. Whereas the  $\pi$ -electron core plays a primary role in the packing motif via  $\pi$ - $\pi$  and subsequent interactions such as  $C-H\cdots\pi$  interaction, side-chain substituents can finely tune the packing structure and intermolecular  $\pi$ -orbital overlaps. In addition, the substituents may contribute to charge transport by modulating the thermal fluctuation of  $\pi$ -orbital overlaps. Hence, it is of great importance for high-performance OSCs to understand distinct roles of  $\pi$ -electron core and side-chain substituents in packing structures and charge-transport properties. In this work, we comparatively studied two analogous n-type OSCs with phenyl- or cyclohexyl-terminated substituents. The solution-processed single-crystal thin-film transistor based on the cyclohexyl derivative exhibited the best electron mobility of 2.3 cm<sup>2</sup> V<sup>-1</sup> s<sup>-1</sup>, which is slightly lower than that based on the phenyl counterpart. While both derivatives form the analogous packing structures, only the phenyl derivative shows weak  $C-H\cdots\pi$  intermolecular interactions between neighboring phenyl groups. Hence, the higher mobility is attributed to suppressed molecular motions owing to the phenyl-to-phenyl interactions, which was successfully revealed by molecular dynamics simulations. Therefore, a potential impact of substituent-engineered molecular design is presented.

## **ARTICLE**

Received 00th January 20xx, Accepted 00th January 20xx

DOI: 10.1039/x0xx000000x

# Phenyl- versus cyclohexyl-terminated substituents: Comparative study on aggregated structures and electron-transport properties in n-type organic semiconductors

Shohei Kumagai,<sup>a,b</sup>\* Takeru Koguma,<sup>b</sup> Yutaro Arai,<sup>c</sup> Go Watanabe,<sup>d,e</sup> Hiroyuki Ishii,<sup>f</sup> Jun Takeya,<sup>b,c</sup> Toshihiro Okamoto<sup>a,b,c</sup>\*

Substituent engineering is a key route to high-performance functional molecular materials in the same way as a development of  $\pi$ -electron core for organic (opto-)electronics. Here we demonstrate a comparative study between aromatic phenyl- and aliphatic cyclohexyl-terminated side-chain substituents on an electron-deficient  $\pi$ -electron core, 3,4,9,10-benzo[de]isoquinolino[1,8-gh]quinolinetetracarboxylic diimide (BQQDI), to get insights into the impact of intermolecular interactions between the substituents in the solid states on high-performance electron-transport properties. In the BQQDI system, both phenyl- and cyclohexyl-terminated ethyl substituents show the similar packing structures, demonstrating unobvious impacts of terminal groups. However, solution-processed single-crystal transistor studies revealed a relatively low electron mobility of cyclohexyl-terminated BQQDI. Based on molecular dynamics simulation, we attribute this discrepancy to dynamic molecular motions coupled with electronic coupling in the solid states. While phenyl groups in the phenylethyl substituent show intermolecular C-H··· $\pi$  interactions which lead to less dynamic motions, the cyclohexyl counterpart does not show any specific intermolecular interactions. Hence, a low-dynamic feature thanks to inter-side-chain interactions is promising for excellent charge-transport properties. The present findings underline the crucial role of interactions between substituents in the development of organic materials via side-chain-engineered control of the solid-state dynamic motions.

#### 1. Introduction

The aggregated structure is a key factor of functional molecular materials. In charge-transporting organic semiconductors (OSCs), the solid-state packing structure of  $\pi$ -electron cores ( $\pi$ -cores) is particularly important since the charge transport is governed by the intermolecular overlap of  $\pi$ -orbitals.<sup>1,2</sup> Whereas  $\pi$ -cores principally tend to form  $\pi$ -stacking structures, competitive intermolecular (e.g.,  $C-H\cdots\pi$ ) interactions may induce the herringbone packing motif.<sup>3–5</sup> On the other hand, an incorporation of heteroatoms, such as O, N, S and halogen, into

the  $\pi$ -core further complicates the resulting packing motif due to additional intermolecular interactions, such as hydrogen bonds, <sup>6,7</sup> and the polarization of  $\pi$ -core, <sup>8</sup> resulting in the slipped/cofacial  $\pi$ -stacking motif, brickwork and so on. As such, the  $\pi$ -cores could play a basic role in the packing structure and charge-transport capability of OSCs.

Besides, recent progress in OSCs demonstrates molecular structures composed of not only a  $\pi$ -core but also side-chain substituents, 9,10 the latter of which primarily solubilize  $\pi$ conjugated molecules for solution-processable electronics. 11-13 In this context, aliphatic alkyl chains are flequently adopted for OSCs due to their flexilibility and affinity for organic solvents conventionally used for aromatic compounds, making both synthesis and device fabrication convenient. In addition, the side-chain substituents are cricial for the packing structure, ranging from fine-tuning to drastic rearrangements, and thus for charge transport capability. 12,14-17 Furthermore, the sidechain substituents could impact suppressing thermally excited molecular motions which attribute to a fluctuation of intermolecular electronic coupling, namely, dynamic disorder and non-local electron-phonon couplings, leading to higher charge-carrier mobilities. 18-20

Although alkyl substituents play an appropriate role in high-mobility hole-transporting (p-type) OSCs with the herringbone motif,  $^{18,19,21}$  the role is not versatile for an enormous range of  $\pi$ -cores. For example, some of electron-transporting (n-type)

<sup>&</sup>lt;sup>a</sup> Department of Chemical Science and Engineering, School of Materials and Chemical Technology, Tokyo Institute of Technology, 4259-G1-7 Nagatsuta, Midori-ku, Yokohama 226-8502, Japan. E-mail: kumagai.s.am@m.titech.ac.jp; tokamoto@cap.mac.titech.ac.jp

b Material Innovation Research Center (MIRC) and Department of Advanced Materials Science, Graduate School of Frontier Sciences, The University of Tokyo, 5-1-5 Kashiwanoha, Kashiwa, Chiba 277-8561, Japan

<sup>&</sup>lt;sup>c</sup> Department of Applied Chemistry, Graduate School of Engineering, The University of Tokyo, 7-3-1 Hongo, Bunkyo-ku, Tokyo 113-8656, Japan

<sup>&</sup>lt;sup>d</sup> Department of Data Science, School of Frontier Engineering, Kitasato University, 1-15-1 Kitazato, Minami-ku, Sagamihara, Kanagawa 252-0373, Japan

E. Kanagawa Institute of Industrial Science and Technology (KISTEC), 705-1 Shimoimaizumi, Ebina, Kanagawa 243-0435, Japan

f. Department of Applied Physics, Faculty of Pure and Applied Sciences, University of Tsukuba, 1-1-1 Tennodai, Tsukuba, Ibaraki 305-8573, Japan

<sup>†</sup> Footnotes relating to the title and/or authors should appear here. Electronic Supplementary Information (ESI) available: [details of any supplementary information available should be included here]. See DOI: 10.1039/x0xx00000x

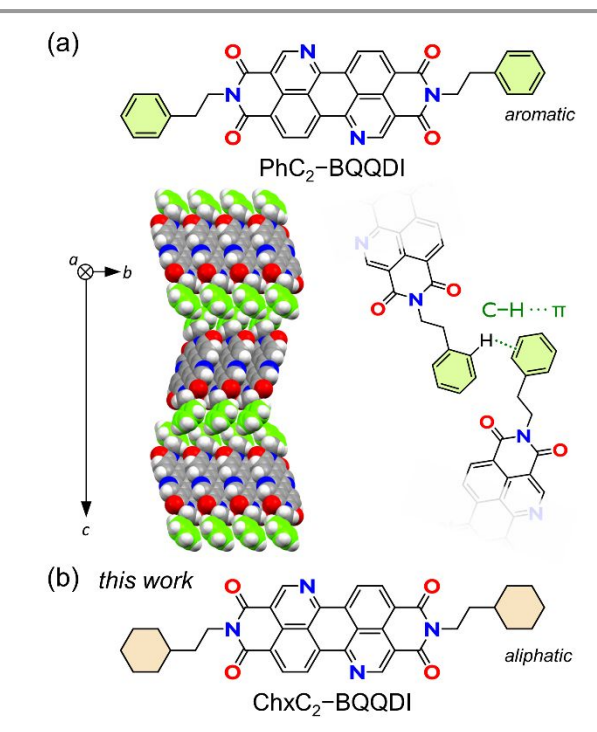


Fig. 1. Research target in this work. (a) Chemical and crystal structures of phenylterminated PhC<sub>2</sub>–BQQDI (CCDC: 1938483), and schematic drawing of interlayer C–H··· $\pi$  interaction between phenyl groups. C, gray and green (for phenyl group); H, white; N, blue; O, red. (b) Chemical structure of cyclohexyl-terminated ChxC<sub>2</sub>–BQQDI featured in this work.

OSCs demonstrated high electron mobilities with the brickwork packing motif, which is organized by fluoroalkyl or cyclohexyl substituents rather than alkyl ones.  $^{22-24}$  Hence, it is necessary to clarify distinct roles of  $\pi\text{-core}$  and side-chain substituents in packing structure and charge-transport properties, which leads to an opportunity of side-chain substituent engineering to achieve the optimal packing structure for high OSC performances with each designed  $\pi\text{-core}.$ 

Our group has recently developed n-type OSCs based on 3,4,9,10-benzo[de]isoquinolino[1,8-gh]quinoline diimide (BQQDI)  $\pi$ -core.<sup>25,26</sup> A typical characteristic of BQQDI derivatives is the layered brickwork structure triggered by intermolecular C-H···O and C-H···N attractive interactions in the lateral direction of  $\pi$ -core. In the BQQDI family reported, 2phenylethyl-substituted derivative (PhC2-BQQDI) exhibits a high electron mobility up to 3.0  $\mbox{cm}^2~\mbox{V}^{-1}~\mbox{s}^{-1}$  under ambient atmosphere.25 In the layered brickwork structure of PhC<sub>2</sub>-BQQDI, the terminal phenyl groups further contribute to  $C-H\cdots\pi$  interactions (Fig. 1a). This  $C-H\cdots\pi$  interaction between substituents could suppress thermal motion of molecules in the aggregated structure in cooperation with the C-H···O and C-H···N interactions between  $\pi$ -cores, resulting in suppressed dynamic disorder which is a detrimental factor decreasing the charge-carrier mobility.<sup>27,28</sup> Although the ethyl linker has been modified with different alkyl chain lengths, 29 it is also interesting to study an impact of the terminal phenyl group for future solution-processable OSC developments.

In this work, we have studied the crucial role of terminal phenyl groups in  $PhC_2$ -BQQDI. For this, 2-cyclohexylethyl-substituted

BQQDI (ChxC<sub>2</sub>–BQQDI) was synthesized because the aliphatic cyclohexyl ring is the representative opponent of phenyl group<sup>24,30–34</sup> and promises a lack of the aforementioned C–H··· $\pi$  interactions (Fig. 1b). Through comparative studies on crystallography and charge-transport property, the cyclohexyl replacement was not so influential for the crystal packing; however, molecular dynamics simulation revealed that the absence of C–H··· $\pi$  interaction in ChxC<sub>2</sub>–BQQDI could cause relatively large thermal motions and dynamic disorder in the crystalline states, which leads to a lower electron mobility than PhC<sub>2</sub>–BQQDI, while it is still high as 2.3 cm² V<sup>-1</sup> s<sup>-1</sup>. Hence, this paper shows a significant role of intermolecular interactions between side-chain substituents beared on the  $\pi$ -core in enhancing charge-transport properties through a suppression of dynamic molecular motions in crystalline molecular solids.

#### 2. Experimental

#### 2.1. Materials

Benzo[de]isoquinolino[1,8-gh]quinolinetetracarboxylic dianhydride (BQQ-TCDA) and PhC<sub>2</sub>-BQQDI was prepared according to the literature.<sup>25</sup> The other reagents and solvents were purchased and used without further purification, whereas o-dichlorobenzene was purified by using a solvent purification system (GlassContour, Nikko Hansen Co., Ltd.) prior to use.

#### 2.2. Instruments

 $^1$ H nuclear magnetic resonance (NMR) spectra were acquired with a JEOL ECS400 spectrometer (400 MHz) in deuterated sulfuric acid (D $_2$ SO $_4$ ) at 25 °C. Chemical shifts are reported in  $\delta$  ppm.  $^1$ H NMR spectra are referenced to residual protons of sulfuric acid ( $\delta$  10.90 ppm) as an internal standard. The data are presented in the following format: chemical shift, multiplicity (s = singlet, d = doublet, br = broad), coupling constant in Hertz (Hz), signal area integration in natural numbers. Elemental analysis was performed on a J-Science Lab JM10 CHN analyzer.

#### 2.3. X-ray crystallography

Single-crystal X-ray diffraction data were collected on a Rigaku R-AXIS RAPID II imaging plate diffractometer with  $CuK\alpha$  radiation ( $\lambda$  = 1.54187 Å). The structures were solved by direct methods (SHELXT<sup>35</sup> (Ver. 2014/4)) and refined by full-matrix least-squares procedures on  $F^2$  for all reflections (SHELXL<sup>36</sup> (Ver. 2014/7)) by using CrystalStructure interface (Rigaku (Ver. 4.2.2)). While all hydrogen atoms were placed at calculated positions, all other atoms were refined anisotropically. Crystallographic data have been deposited in the Cambridge Crystallographic Data Centre as supplementary publication. The data can be obtained free of charge from the Cambridge Crystallographic Data Centre via www.ccdc.cam.ac.uk/data\_request/cif (CCDC 2232687).

#### 2.4. Quantum chemical calculations

The intermolecular interaction energies between pairs of adjacent molecules were obtained at the M06-2X/6-31++G(d,p)

Journal Name ARTICLE

level of density functional theory (DFT) with counterpoise correction<sup>37,38</sup> for the basis set superposition error. Transfer integrals between LUMO of adjacent molecules were calculated at the PBEPBE/6-31G(d) level of DFT.

#### 2.5. Band calculation

Band calculation was conducted by the tight-binding approximation. Effective masses of electrons were calculated from the curvature of the LUMO-band bottom according to the following equation:

$$\frac{1}{m^*} = \frac{1}{\hbar^2 \partial k^2}$$
 (1

where  $m^*$  is the effective mass,  $\hbar$  the Dirac's constant, E the energy, k the wave vector. In band theory, a charge-carrier mobility ( $\mu$ ) is expressed by the following equation:<sup>39</sup>

$$\mu = q\tau/m^* \tag{2}$$

where q and  $\tau$  are the elementary charge and relaxation time of charge carriers, respectively.

#### 2.6. Molecular dynamics simulation

All-atom molecular dynamics (MD) simulations were performed using GROMACS 2016.3. The generalized Amber force field<sup>40</sup> parameters were used for the force field parameters of both  $ChxC_2$ –BQQDI and  $PhC_2$ –BQQDI and their atomic charges were calculated using the restrained electrostatic potential (RESP)<sup>41</sup> methodology based on DFT calculations (B3LYP/6-31G(d)) using the GAUSSIAN09 program.<sup>42</sup> The time step was set to 1 fs. The long-range Coulomb interactions were calculated with the smooth particle-mesh Ewald (PME)<sup>43</sup> method with a grid spacing of 0.30 nm. The real space cutoff for both Coulomb and van der Waals interactions was 1.2 nm. The *B*-factors were calculated by the following equation:

$$B = \frac{8}{3}\pi^2 \Delta_i^2 \qquad (3)$$

where  $\Delta_i$  is the root mean square fluctuations (RMSF) of atom i. The RMSF values were estimated by the following equation:

$$\Delta_i = \sqrt{\frac{1}{T} \sum_{j=1}^{T} |\boldsymbol{r}_i(t_j) - \overline{\boldsymbol{r}}_i|^2}$$
 (4)

where T is the time step,  $r_i(t_j)$  is the position coordinate of atom i, and  $\overline{r}_i$  is the average of  $r_i(t_j)$ .  $10 \times 10 \times 3$  super cell including 600 molecules was prepared based on the single crystal structure, and 5 and 50 ns MD runs were sequentially performed by the number–temperature–volume (NTV) and the number–temperature–pressure (NTP) ensembles, respectively, at the temperatures same as the crystallographic data (295 and 296 K for ChxC<sub>2</sub>–BQQDI and PhC<sub>2</sub>–BQQDI, respectively). The pre-equilibrium NTV run was carried out by using the Berendsen<sup>44</sup> thermostat, whereas the NTP process was conducted by using and the Nosé-Hoover<sup>45–47</sup> thermostat and Parrinello-Rahman barostat.<sup>48</sup>

# 2.7. Synthesis of *N,N'*-di(2-cyclohexylethyl)-3,4,9,10-benzo[*de*]isoquinolino[1,8-*gh*]quinolinetetracarboxylic diimide (ChxC<sub>2</sub>-BQQDI)

To a Schlenk flask was charged BQQ-TCDA (200 mg; 0.51 mmol), 2-cyclohexylethylamine (0.22 mL; 1.52 mmol), propionic acid (3.80 mL; 50.8 mmol) and o-dichlorobenzene (17 mL) and sealed. The mixture was stirred at 130 °C for 5 h under an argon atmosphere to yield red-brown suspension. The precipitates were collected by suction filtration, washed with excess methanol, and dried in vacuo. After recrystallization from odichlorobenzene (0.143 g L<sup>-1</sup> dissolved at 150 °C), 271 mg of redbrown solids were collected (yield: 87% based on BQQ-TCDA). Further purification was performed by sublimation under vacuum for compound characterization and device studies. <sup>1</sup>H NMR (400 MHz,  $D_2SO_4$ , 25 °C):  $\delta$  9.56 (s, 2H, ArH), 9.37 (d, J = 8.4Hz, 2H, ArH), 9.31 (d, J = 8.0 Hz, 2H, ArH), 4.18 (br, 4H, NCH <), 1.72 (br, 4H, -CH<sub>2</sub>-), 1.65-1.56 (br, 10H, -CH<sub>2</sub>-), 1.37 (br, 2H, -CH<sub>2</sub>-), 1.24-1.08 (br, 6H, -CH<sub>2</sub>-), 1.00-0.92 (br, 4H, -CH<sub>2</sub>-). <sup>13</sup>C NMR could not be obtained due to poor solubility. Anal. Calcd. for C<sub>38</sub>H<sub>36</sub>N<sub>4</sub>O<sub>4</sub>: C, 74.49; H, 5.92; N, 9.14. Found: C, 74.51; H, 5.99; N, 9.11.

#### 2.8. Device fabrication and characterization

Single-crystal OTFTs were fabricated in the bottom-gate/top-contact geometry. An  $n^{++}$ -Si/SiO<sub>2</sub> (200 nm) wafer encapsulated with a thermally cross-linked insulating polymer AL-X601 (AGC Inc.; 40 nm) was used as the substrate, where  $n^{++}$ -Si and SiO<sub>2</sub>/AL-X601 bilayer act as the gate electrode and gate dielectric layer, respectively. Single-crystalline thin films of ChxC<sub>2</sub>–BQQDI were solution-crystallized by the edge casting method<sup>49</sup> from its 1-methylnaphthalene solution. Au layers (40 nm) were vacuum-deposited onto the thin films through a metal shadow mask as the top-contact source and drain electrodes, followed by laser etching to afford the single-crystal OTFTs. A post-annealing process at 100 °C was conducted for 2 h under vacuum prior to electrical evaluations.

Electrical evaluations were carried out with a Keithley 4200-SCS semiconductor parameter analyzer under ambient atmosphere. Electron mobilities in the linear and saturation regimes were estimated the conventional equation:

$$I_{\rm D} = \frac{W\mu_{\rm lin}C_{\rm i}}{L}V_{\rm D}(V_{\rm G} - V_{\rm th}) \qquad (5)$$

and

$$\sqrt{I_{\rm D}} = \sqrt{\frac{W\mu_{\rm sat}C_{\rm i}}{2L}}(V_{\rm G} - V_{\rm th}) \tag{6}$$

respectively, where W is the channel width, L the channel length,  $C_i$  the gate capacitance per unit area ( $C_i$  = 14.2 nF cm<sup>-2</sup> measured by the Keithley 4200-SCS),  $I_D$  the drain current,  $V_D$  the drain voltage,  $V_{\rm th}$  the threshold voltage, and  $\mu_{\rm lin}$  and  $\mu_{\rm sat}$  the electron mobility in the linear and saturation regimes, respectively.

#### 3. Results and discussion

#### 3.1. Synthesis, X-ray crystallography and transport calculations

ChxC<sub>2</sub>-BQQDI was prepared by the similar way as PhC<sub>2</sub>-BQQDI (Scheme S1, ESI).<sup>25</sup> A red plate-like single crystal of ChxC<sub>2</sub>-BQQDI enough for X-ray crystallography was obtained by

recrystallization from nitrobenzene. The X-ray single-crystal structure of ChxC2-BQQDI is shown in Fig. 2, where the

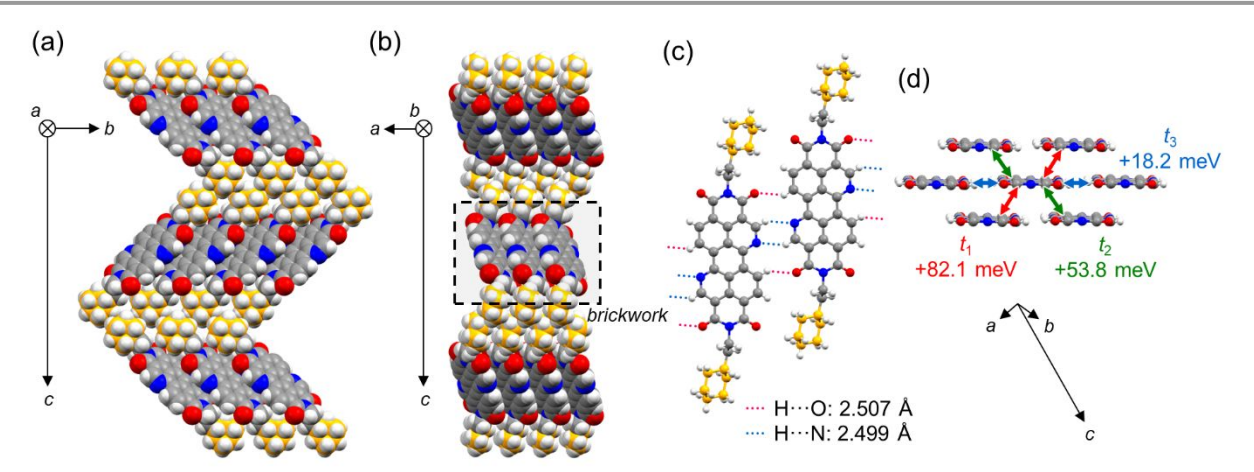


Fig. 2. Single-crystal crystal structure of ChxC<sub>2</sub>-BQQDI. (a, b) Packing structures viewed along the *a*- and *b*-axes. (c) Intermolecular C-H···O and C-H···O interactions in the lateral direction. van der Waals radius<sup>50</sup>: H, 1.20 Å; N, 1.55 Å; O, 1.52 Å. Close contacts are estimated relative to a sum of the van der Waals radii. (d) Geometry of the brickwork structure and transfer integrals corresponding to the layer highlighted by a black-lined square in (b). C, orange and gray (for cyclohexyl moiety and the others, respectively); H, white; N, blue; O, red.

crystallographic system of monoclinic  $P2_1/n$  resembles that of PhC<sub>2</sub>-BQQDI,<sup>25</sup> whereas the a- and b-axes are exchanged (Table S1). Thus, ChxC2-BQQDI exhibits the brickwork aggregated structure supported by the attractive C-H···N and C-H···O interactions between the BQQDI  $\pi$ -cores with close H···O and H···N contacts (2.507 and 2.499 Å, respectively) (Fig. 2c), despite a lack of specific weak intermolecular C–H… $\pi$  interactions between phenyl groups observed in PhC<sub>2</sub>-BQQDI (Fig. 1a). This fact can reveal that the attractive C-H···N and C-H···O interactions and the volumetric filling arising from the similar molecular structures are significant for their packing structures. An apparent interdigitation of 2-phenylethyl substituents is loosen in ChxC2-BQQDI, leading to ~10% increase in lattice length in the c-axis while the comparable dimensions in the abplane. The force constant for the laterally aligned ChxC<sub>2</sub>-BQQDI dimer is calculated to be -8.45 kcal mol<sup>-1</sup>, which is comparable to that for PhC<sub>2</sub>-BQQDI (-8.48 kcal mol<sup>-1</sup>)<sup>25</sup> regardless of their different substituents. The similar aggregated structures are also revealed by the short- and long-axis misalignments in  $\boldsymbol{\pi}\text{--}$ stacked BQQDI skeletons (Figs. S3a and S3b, ESI). The long-axis misalignments ( $d_{y1}$  and  $d_{y2}$ ) are +1.00 and +5.47 Å for ChxC<sub>2</sub>-BQQDI, whereas +1.01 and +5.51 Å for PhC<sub>2</sub>-BQQDI, respectively, showing comparable values. As well, the  $\pi\text{-}\pi$ distances  $d_{\pi 1}$  and  $d_{\pi 2}$  are also comparable between ChxC<sub>2</sub>-BQQDI (3.31 and 3.24 Å, respectively) and PhC<sub>2</sub>-BQQDI (3.30 and 3.25 Å, respectively). On the other hand, the shortaxis misalignments ( $d_{x1}$  and  $d_{x2}$ ) show a slight mismatch. In ChxC<sub>2</sub>-BQQDI,  $d_{x1}$  and  $d_{x2}$  are -3.57 and +4.39 Å, respectively, which are smaller than corresponding those values in  $PhC_2$ -BQQDI (-3.68 and +5.14 Å).<sup>29</sup> That is,  $ChxC_2$ -BQQDI demonstrates larger geometrical overlaps of the BQQDI  $\pi$ -cores than PhC2-BQQDI. However, transfer integral calculations suggested a slight reduction of the LUMO overlaps in ChxC<sub>2</sub>-BQQDI than in PhC<sub>2</sub>-BQQDI. Despite their comparable transfer integrals for the lateral direction  $(t_3)$  being +18 meV,

those for the  $\pi$ -stacked dimers ( $t_1$  and  $t_2$ ) are +82.1 and +53.8 meV, respectively, for ChxC<sub>2</sub>–BQQDI, which are slightly smaller than those for PhC<sub>2</sub>–BQQDI (+90.7 and +58.5 meV).<sup>25</sup> This difference is attributed to the difference in the short-axis misalignments, which direction crosses the major nodes of LUMOs of the BQQDI  $\pi$ -core (Fig. S3c, ESI).

# **3.2.** Computational insights into molecular conformation in single crystal

Here we would like to address the relationship of molecular conformation between crystal structure and geometry optimization by quantum chemical calculation to consider the engineering ability of aggregated structure by adopting the 2cyclohexylethyl substituent. In Fig. 3, single-molecule geometries are compared between the X-ray diffraction (XRD) analysis at room temperature and a geometry optimization by the B3LYP/6-31+G(d) level of DFT, where both ChxC2-BQQDI and PhC2-BQQDI show good similarities at a glance. As summarized in Table 1, for more details, the differences of some specific geometrical parameters between XRD and DFT results are smaller for ChxC<sub>2</sub>-BQQDI than those for PhC<sub>2</sub>-BQQDI. This might be attributed to the general steric effects in aliphatic alkyl chains, which subjects the 2-cyclohexylethyl substituent to an almost fixed conformation, in contrast to the phenethyl substituent having less intramolecular steric repulsions. Yet, in reality, the argument for the 2-cyclohexylethyl group depends on the  $\pi$ -core. As the representative, a crystal structure of 2cyclohexylethyl substituted naphtho[2,3-b:6,7-b']dithiophene diimide (NDTI) has been reported by Takimiya and co-workers.51 In this case, the deviation between XRD and DFT works is far remarkable (Fig. S4 and Table S2, ESI). Therefore, the 2cyclohexylethyl-substituted ChxC2-BQQDI brushes up a chemistry of aggregated structures of BQQDI derivatives and provides an interesting insight into 2-cyclohexyl substituent for organic semiconductors.

Journal Name ARTICLE

#### 3.3. Solution-crystallized single-crystal transistors

Charge-transport properties of  $ChxC_2$ -BQQDI were investigated by solution-crystallized single-crystal OTFTs. The OTFTs were

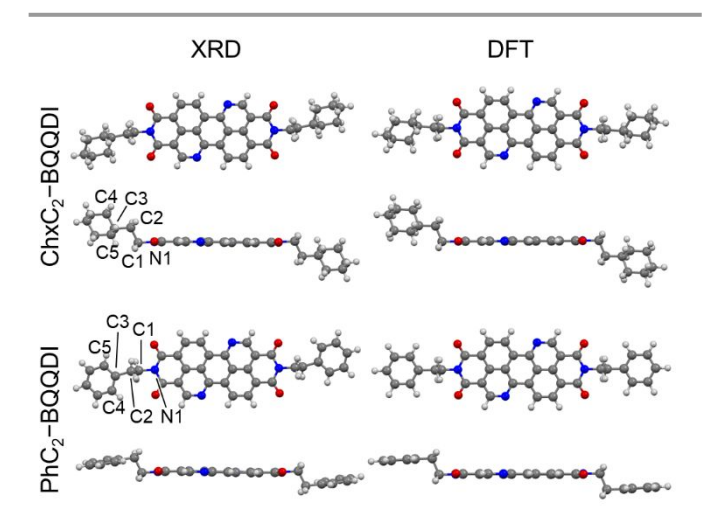


Fig. 3. Comparison of single-molecule geometry between XRD and DFT. C, gray; H, white; N, blue; O, red.

Table 1. Summary of bond and torsion angles for ChxC2-BQQDI and PhC2-BQQDI.

Measured angle	ChxC <sub>2</sub> -BQQDI		PhC₂-BQQDI	
	XRD	DFT	XRD	DFT
Bond angle ∠(N1-C1-C2) (°)	113.2	112.2	113.0	112.4
Bond angle ∠(C1-C2-C3) (°)	112.4	113.7	109.1	111.4
Torsion angle ∠(N1-C1-C2-C3) (°)	11.3	4.1	14.9	0.0
Torsion angle ∠(C1-C2-C3-C4) (°)	11.3	11.0	80.1	89.3
Torsion angle ∠(C1-C2-C3-C5) (°)	67.7	67.1	97.2	89.2

fabricated in a bottom-gate/top-contact geometry with gold source and drain electrodes (Fig. 4a). Single-crystal channels were edged by means of laser ablation to assess the chargecarrier mobility properly (Fig. 4b). As shown in Figs. 4c-f, ChxC2-BQQDI exhibits typical n-channel OTFT characteristics under ambient atmosphere. The best device exhibited high electron mobilities of 1.92 and 2.35 cm<sup>2</sup> V<sup>-1</sup> s<sup>-1</sup> in the linear ( $\mu_{lin}$ ) and saturation regimes ( $\mu_{sat}$ ), respectively, where the  $\mu_{sat}$  value is slightly lower than that of PhC<sub>2</sub>-BQQDI reported (3.0 cm<sup>2</sup> V<sup>-1</sup> s<sup>-1</sup>)<sup>25</sup>. XRD measurement on the OTFT assigned the channel direction to [0 1 0] (i.e., the b-axis direction) (Fig. S5, ESI). To consider theoretical electron-transport capabilities with anisotropy, band calculations were further carried out. The inverse of effective mass of electrons  $(m^*)^{-1}$  within the ab plane is azimuthally plotted in Fig. S6, ESI, where horizontal and vertical directions correspond to [0 1 0] and [1 0 0] directions in the crystal structures of both derivatives. Although the overall size of a peanut-like  $(m^*)^{-1}$  distribution is larger for PhC<sub>2</sub>-BQQDI than that for ChxC2-BQQDI due to their relative transfer

integrals, the  $(m^*)^{-1}$  value along the [0 1 0] direction, which corresponds to the channel direction of solution-crystallized single-crystal OTFTs based on both derivatives, is larger in  $ChxC_2$ -BQQDI. Since a charge-carrier mobility is proportional to

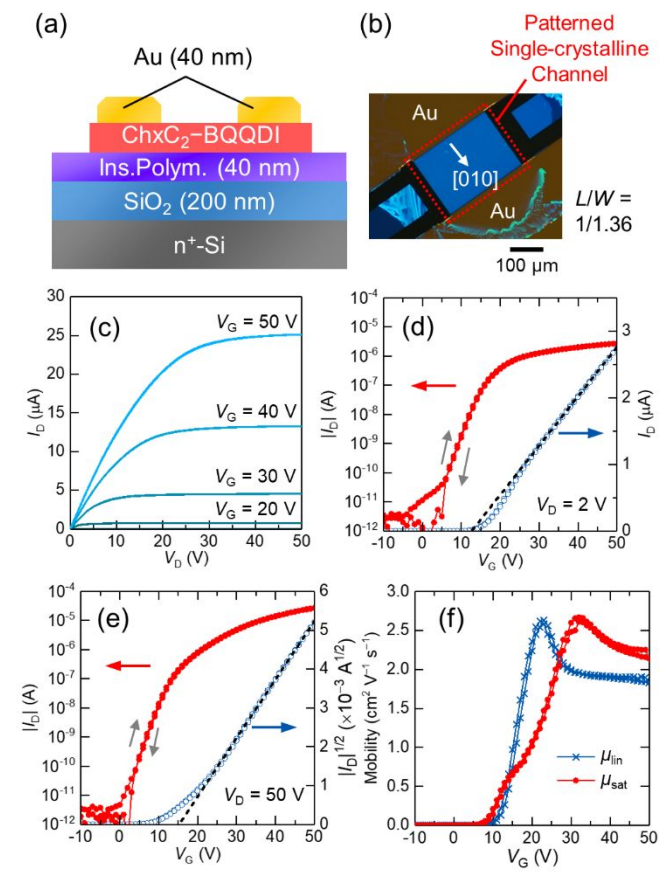


Fig. 4. Solution-crystallized single-crystal OTFT based on ChxC<sub>2</sub>–BQQDI. (a) Schematic device structure. (b) Cross-polarized microscopy image. Channel length  $\it L$  is 200  $\mu m$ . (c) Output and (d-e) transfer characteristics. (f)  $\it V_G$ -dependent electron mobility.

 $(m^*)^{-1}$  in band theory (Eq. 2), these results imply that  $ChxC_2$ -BQQDI could exhibit a higher electron mobility than  $PhC_2$ -BQQDI.

#### 3.4. Molecular dynamics simulation and dynamic disorder

To study the inconsistency between the calculational and experimental results, MD simulations were performed on  $ChxC_2$ –BQQDI based on the crystal structure. Figs. 5a and 5b show *B*-factor distributions after MD run, which depicts the isotropic thermal fluctuations resolved into atoms. The MD simulation of  $ChxC_2$ –BQQDI revealed a effectively suppressed thermal motion of BQQDI  $\pi$ -core and ethyl moieties (colored exclusively by blue) similarly to  $PhC_2$ –BQQDI (Figs. S8a and S8b and Table S3, ESI) owing to the lateral C–H····N and C–H····O attractive interactions. <sup>25</sup> On the other hand, cyclohexyl rings are regularly colored by light blue, suggesting their potential thermal disordering due to the absence of specific intermolecular interactions. In particular, C atoms at 2-, 3-, 5- and 6-positions of cyclohexyl ring in a few  $ChxC_2$ –BQQDI molecules within the supercell are highlighted by red color (Fig.

5b), whose *B*-factors exceed 30  $Å^2$ . This irregular cyclohexyl rings are associated with a rotation of cyclohexyl ring around an

axis linking C atoms at 1- and 4-positions (Fig. 5c). Although it is curious if such rotations occur in a real crystal, this result would

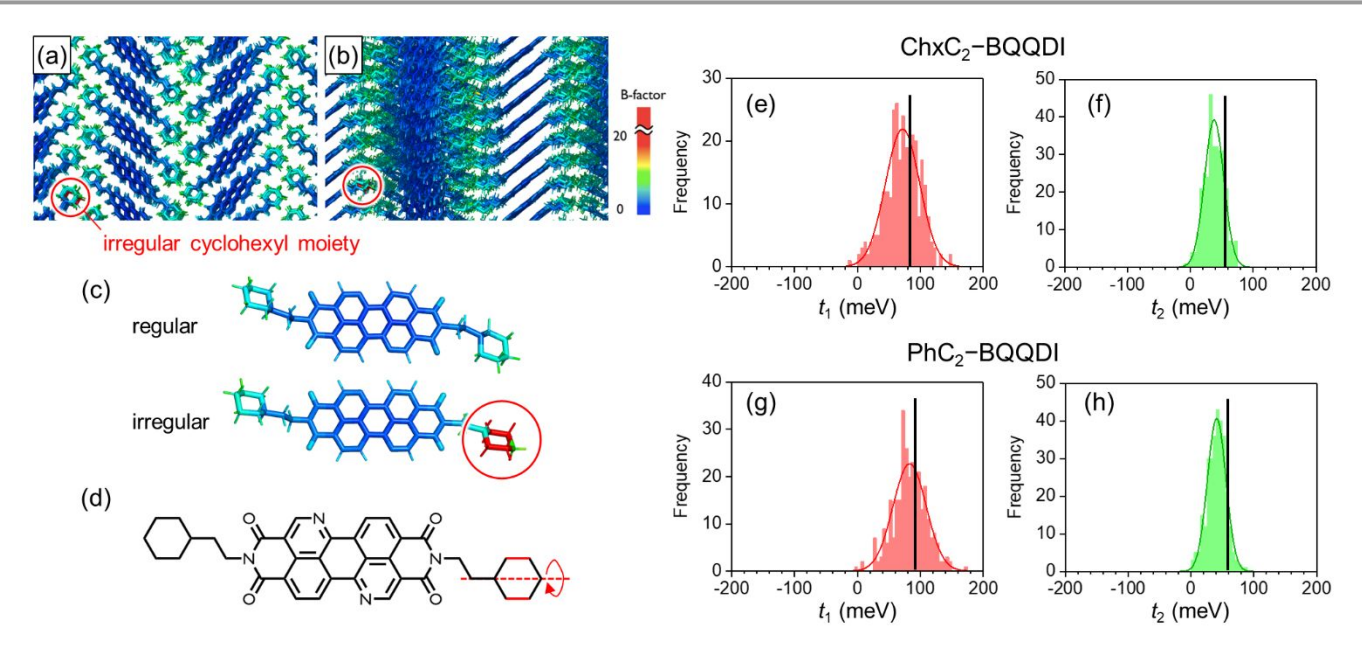


Fig. 5. MD simulation for  $ChxC_2$ –BQQDI. (a-b) Color-coded *B*-factor distribution (unit: Å<sup>2</sup>) obtained from the trajectory of the crystal structure during the last 10 ns of 50 ns MD runs at 295 K. (c) Representative molecules extracted from (a) with the regular and irregular *B*-factor distributions at the cyclohexyl moiety. (d) Schematic depiction of a rotation of cyclohexyl moiety corresponding to the irregular molecule in (c). (e-f) Statistics of transfer integrals  $t_1$  and  $t_2$  based on the MD simulation of  $ChxC_2$ –BQQDI, and (g-h) of  $PhC_2$ –BQQDI. Red and blue solids lines show the corresponding normal distributions. Thick black line indicates the transfer integrals calculated from the crystal structure.

possibly suggest local structural disorders and defects in the single crystals. Besides, in comparison with the single crystal data, the unit cell volume after the MD simulations was more expanded in ChxC<sub>2</sub>-BQQDI (~1.4%) than in PhC<sub>2</sub>-BQQDI (~0.6%) (Figure S7), suggesting an effectiveness of the C–H $\cdots\pi$ interactions in the robust aggregated structure of PhC<sub>2</sub>-BQQDI. In addition, the thermal molecular motions are coupled with a dynamic variation of transfer integrals, i.e., dynamic disorder.<sup>27,28</sup> The degree of dynamic disorder was estimated by calculating a population of transfer integrals after MD runs; in ChxC<sub>2</sub>-BQQDI, the average transfer integral values ( $t_{avg}$ ) corresponding to  $t_1$ ,  $t_2$  and  $t_3$  are 71.6 (27.2), 37.8 (15.3) and 11.6 (2.6) meV, respectively, where the value in the parentheses indicates a standard deviation ( $\sigma$ ) (Figs. 5e-f and S7c, and Table S4, ESI). Resulting coefficient of variation ( $\sigma/t_{avg}$ ) is calculated as a brief measure of dynamic disorder to be 0.38, 0.41 and 0.22. On the other hand, for PhC<sub>2</sub>-BQQDI, corresponding  $\sigma/t_{avg}$ values are 0.32, 0.36 and 0.23 (Figs. 5g-h and S7d, and Table S4, ESI) (note that these  $t_{\mathrm{avg}}$  and  $\sigma$  values are slightly different from those in ref. 25 because of the sophisticated parameters for simulation). Hence, ChxC<sub>2</sub>-BQQDI could show larger dynamic disorder to lead to lower electron mobilities than PhC2-BQQDI, which is consistent with our experimental results.

# 4. Conclusions

Here we reported a comparative study on a 2-phenylethylsubstituted high-performance n-type OSC PhC2-BQQDI and its 2-cyclohexylethyl-substituted analogue, ChxC<sub>2</sub>-BQQDI. ChxC2-BQQDI bearing only aliphatic hydrocarbons constructs the very similar aggregated structure with PhC2-BQQDI which crystallizes in the layered brickwork structure supported by  $C-H\cdots\pi$  interactions between phenyl groups. Solutioncrystallized single-crystal transistors based on ChxC2-BQQDI demonstrated a high electron mobility of 2.3 cm<sup>2</sup> V<sup>-1</sup> s<sup>-1</sup> in air. This mobility is lower than that of PhC2-BQQDI reported, whereas theoretical calculations suggest higher electron mobility of ChxC2-BQQDI. Further analysis by means of MD simulation revealed more serious dynamic disorder of ChxC<sub>2</sub>-BQQDI, demonstrating a crucial role of interactions between substituents in charge-carrier transport in molecular semiconductors. The present results will be helpful for the materials design of crystalline, high-performance OSCs by sidechain-engineered suppression of molecular motions.

#### **Conflicts of interest**

There are no conflicts to declare.

#### Acknowledgements

The authors acknowledge AGC Inc. for supplying AL-X601. This project was partially supported by the JST-PRESTO and JST-

6 | J. Name., 2012, **00**, 1-3

This journal is © The Royal Society of Chemistry 20xx

Journal Name ARTICLE

CREST programs "Scientific Innovation for Energy Harvesting Technology" (nos. JPMJPR17R2 and JPMJCR21Q1) and "Exploring Innovative Materials in Unknown Search Space" (no. JPMJCR21O3) by JSPS KAKENHI (grant nos. JP18H01856, JP19H05716, JP19H05718, JP22K14743, and JP24H00472).

#### **Notes and references**

- J. L. Brédas, J. P. Calbert, D. A. Da Silva Filho and J. Cornil, *Proc. Natl. Acad. Sci. U. S. A.*, 2002, 99, 5804–5809.
- E. F. Valeev, V. Coropceanu, D. A. Da Silva Filho, S. Salman and J. L. Brédas, J. Am. Chem. Soc., 2006, 128, 9882–9886.
- 3 G. R. Desiraju and A. Gavezzotti, *J. Chem. Soc., Chem. Commun.*, 1989, 621–623.
- 4 B. Schatschneider, J. Phelps and S. Jezowski, CrystEngComm, 2011, 13, 7216–7223.
- 5 M. D. Curtis, J. Cao and J. W. Kampf, *J. Am. Chem. Soc.*, 2004, **126**, 4318–4328.
- 6 E. D. Głowacki, M. Irimia-Vladu, S. Bauer and N. S. Sariciftci, *J. Mater. Chem. B*, 2013, **1**, 3742–3753.
- 7 P. Yu, Y. Zhen, H. Dong and W. Hu, *Chem*, 2019, **5**, 2814–2853
- 8 K. E. Maly, Cryst. Growth Des., 2011, **11**, 5628–5633.
- 9 C. Wang, H. Dong, W. Hu, Y. Liu and D. Zhu, *Chem. Rev.*, 2012, **112**, 2208–2267.
- J. Mei, Y. Diao, A. L. Appleton, L. Fang and Z. Bao, J. Am. Chem. Soc., 2013, 135, 6724–6746.
- H. E. Katz, A. J. Lovinger, J. Johnson, C. Kloc, T. Siegrist, W. Li, Y.-Y. Lin and A. Dodabalapur, *Nature*, 2000, **404**, 478–481.
- J. E. Anthony, J. S. Brooks, D. L. Eaton and S. R. Parkin, J. Am. Chem. Soc., 2001, 123, 9482–9483.
- 13 H. Ebata, T. Izawa, E. Miyazaki, K. Takimiya, M. Ikeda, H. Kuwabara and T. Yui, *J. Am. Chem. Soc.*, 2007, **129**, 15732–15733.
- 14 M. C. R. Delgado, E. Kim, S. Filho and J. Bredas, J. Am. Chem. Soc., 2010, 132, 3375–3387.
- J. Vura-Weis, M. A. Ratner and M. R. Wasielewski, *J. Am. Chem. Soc.*, 2010, **132**, 1738–1739.
- Y. Tsutsui, G. Schweicher, B. Chattopadhyay, T. Sakurai, J. B. Arlin, C. Ruzié, A. Aliev, A. Ciesielski, S. Colella, A. R. Kennedy, V. Lemaur, Y. Olivier, R. Hadji, L. Sanguinet, F. Castet, S. Osella, D. Dudenko, D. Beljonne, J. Cornil, P. Samorì, S. Seki and Y. H. Geerts, Adv. Mater., 2016, 28, 7106–7114.
- C. P. Yu, S. Kumagai, T. Kushida, M. Mitani, C. Mitsui, H. Ishii, J. Takeya and T. Okamoto, *J. Am. Chem. Soc.*, 2022, 144, 11159–11167.
- S. Illig, A. S. Eggeman, A. Troisi, L. Jiang, C. Warwick, M. Nikolka, G. Schweicher, S. G. Yeates, Y. Henri Geerts, J. E. Anthony and H. Sirringhaus, *Nat. Commun.*, 2016, 7, 10736.
- 19 G. Schweicher, G. D'Avino, M. T. Ruggiero, D. J. Harkin, K. Broch, D. Venkateshvaran, G. Liu, A. Richard, C. Ruzié, J. Armstrong, A. R. Kennedy, K. Shankland, K. Takimiya, Y. H.

- Geerts, J. A. Zeitler, S. Fratini and H. Sirringhaus, *Adv. Mater.*, 2019, **31**, 1902407.
- M. A. Dettmann, L. S. R. Cavalcante, C. A. Magdaleno and A. J. Moulé, Adv. Funct. Mater., 2023, 33, 2213370.
- T. Okamoto, C. P. Yu, C. Mitsui, M. Yamagishi, H. Ishii and J. Takeya, *J. Am. Chem. Soc.*, 2020, **142**, 9083–9096.
- T. He, Y. Wu, G. D'Avino, E. Schmidt, M. Stolte, J. Cornil, D. Beljonne, P. P. Ruden, F. Würthner and C. D. Frisbie, Nat. Commun., 2018, 9, 2141.
- 23 M. A. Stoeckel, Y. Olivier, M. Gobbi, D. Dudenko, V. Lemaur, M. Zbiri, A. A. Y. Guilbert, G. D'Avino, F. Liscio, A. Migliori, L. Ortolani, N. Demitri, X. Jin, Y. G. Jeong, A. Liscio, M. V. Nardi, L. Pasquali, L. Razzari, D. Beljonne, P. Samorì and E. Orgiu, Adv. Mater., 2021, 33, 2007870.
- 24 C. P. Yu, N. Kojima, S. Kumagai, T. Kurosawa, H. Ishii, G. Watanabe, J. Takeya and T. Okamoto, *Commun. Chem.*, 2021, **4**, 155.
- T. Okamoto, S. Kumagai, E. Fukuzaki, H. Ishii, G. Watanabe, N. Niitsu, T. Annaka, M. Yamagishi, Y. Tani, H. Sugiura, T. Watanabe, S. Watanabe and J. Takeya, *Sci. Adv.*, 2020, 6, eaaz0632.
- S. Kumagai, H. Ishii, G. Watanabe, C. P. Yu, S. Watanabe, J. Takeya and T. Okamoto, *Acc. Chem. Res.*, 2022, **55**, 660–672.
- A. Troisi and G. Orlandi, *Phys. Rev. Lett.*, 2006, **96**, 086601.
- S. Fratini, S. Ciuchi, D. Mayou, G. T. De Laissardière and A. Troisi, *Nat. Mater.*, 2017, **16**, 998–1002.
- S. Kumagai, H. Ishii, G. Watanabe, T. Annaka, E. Fukuzaki, Y. Tani, H. Sugiura, T. Watanabe, T. Kurosawa, J. Takeya and T. Okamoto, *Chem. Mater.*, 2020, 32, 9115–9125.
- 30 K. Kunal, C. G. Robertson, S. Pawlus, S. F. Hahn and A. P. Sokolov, *Macromolecules*, 2008, **41**, 7232–7238.
- J. M. Torres, C. Wang, E. B. Coughlin, J. P. Bishop, R. A. Register, R. A. Riggleman, C. M. Stafford and B. D. Vogt, *Macromolecules*, 2011, 44, 9040–9045.
- M. Hopkins Hatzopoulos, J. Eastoe, P. J. Dowding, I. Grillo,
   B. Demé, S. E. Rogers, R. Heenan and R. Dyer, *Langmuir*,
   2012, 28, 9332–9340.
- O. Munkhbat, M. Garzoni, K. R. Raghupathi, G. M. Pavan and S. Thayumanavan, *Langmuir*, 2016, 32, 2874–2881.
- 34 T. Yu, M. D. Marquez and T. R. Lee, *Langmuir*, 2022, **38**, 13488–13496.
- 35 G. M. Sheldrick, Acta Crystallogr. Sect. A, 2015, 71, 3–8.
- 36 G. M. Sheldrick, Acta Crystallogr. Sect. C, 2015, 71, 3–8.
- 37 S. F. Boys and F. Bernardi, *Mol. Phys.*, 1970, **19**, 553–566.
- 38 M. W. Schmidt, K. K. Baldridge, J. A. Boatz, S. T. Elbert, M. S. Gordon, J. H. Jensen, S. Koseki, N. Matsunaga, K. A. Nguyen, S. Su, T. L. Windus, M. Dupuis and J. A. Montgomery, J. Comput. Chem., 1993, 14, 1347–1363.
- S. M. Sze, Semiconductor Devices: Physics and Technology,
   Wiley, Hoboken, New Jersey, 2nd ed., 2001.
- 40 J. Wang, R. M. Wolf, J. W. Caldwell, P. A. Kollman and D. A. Case, J. Comput. Chem., 2004, 25, 1157–1174.
- 41 C. I. Bayly, P. Cieplak, W. D. Cornell and P. A. Kollman, *J. Phys. Chem.*, 1993, **97**, 10269–10280.
- M. J. Frisch, G. W. Trucks, H. B. Schlegel, G. E. Scuseria, M.A. Robb, J. R. Cheeseman, G. Scalmani, V. Barone, B.

Mennucci, G. A. Petersson, H. Nakatsuji, M. Caricato, X. Li, H. P. Hratchian, A. F. Izmaylov, J. Bloino, G. Zheng, J. L. Sonnenberg, M. Hada, M. Ehara, K. Toyota, R. Fukuda, J. Hasegawa, M. Ishida, T. Nakajima, Y. Honda, O. Kitao, H. Nakai, T. Vreven, J. A. Montgomery Jr., J. E. Peralta, F. Ogliaro, M. Bearpark, J. J. Heyd, E. Brothers, K. N. Kudin, V. N. Staroverov, R. Kobayashi, J. Normand, K. Raghavachari, A. Rendell, J. C. Burant, S. S. Iyengar, J. Tomasi, M. Cossi, N. Rega, J. M. Millam, M. Klene, J. E. Knox, J. B. Cross, V. Bakken, C. Adamo, J. Jaramillo, R. Gomperts, R. E. Stratmann, O. Yazyev, A. J. Austin, R. Cammi, C. Pomelli, J. W. Ochterski, R. L. Martin, K. Morokuma, V. G. Zakrzewski, G. A. Voth, P. Salvador, J. J. Dannenberg, S. Dapprich, A. D. Daniels, Ö. Farkas, J. B. Foresman, J. V. Ortiz, J. Cioslowski and D. J. Fox, Gaussian 09 (Revision E.01), Gaussian Inc., Pittsburgh, PA, 2009.

- T. Darden, D. York and L. Pedersen, J. Chem. Phys., 1993,98, 10089–10092.
- H. J. C. Berendsen, J. P. M. Postma, W. F. Van Gunsteren, A.
   Dinola and J. R. Haak, J. Chem. Phys., 1984, 81, 3684–3690.
- 45 S. Nosé, *Mol. Phys.*, 1984, **52**, 255–268.
- 46 S. Nosé, J. Chem. Phys., 1984, **81**, 511–519.
- 47 W. G. Hoover, *Phys. Rev. A*, 1985, **31**, 1695–1697.
- 48 M. Parrinello and A. Rahman, J. Appl. Phys., 1981, 52, 7182–7190.
- T. Uemura, Y. Hirose, M. Uno, K. Takimiya and J. Takeya, *Appl. Phys. Express*, 2009, **2**, 111501.
- 50 A. Bondi, J. Phys. Chem., 1964, **68**, 441–451.
- 51 M. Nakano, D. Hashizume and K. Takimiya, *Molecules*, 2016, **21**, 981.

## **Data Availability Statements**

Crystallographic data has been deposited in the Cambridge Crystallographic Data Centre (CCDC) under 2232687 and can be obtained free of charge from the Cambridge Crystallographic Data Centre via www.ccdc.cam.ac.uk/data\_request/cif.